

Folding of Aquaporin 1: Multiple evidence that helix 3 can shift out of the membrane core

Minttu T. Virkki,¹ Nitin Agrawal,² Elin Edsbäcker,¹ Susana Cristobal,^{3,4} Arne Elofsson,^{1*} and Anni Kauko²

¹Department of Biochemistry and Biophysics and Science for Life Laboratory, Stockholm University, Solna SE-171 21, Sweden

²Department of Biosciences, Biochemistry, Åbo Akademi, Turku FI-20520, Finland

³Department of Clinical and Experimental Medicine, Cell Biology, Faculty of Health Science, Linköping University, Linköping, Sweden

⁴Department of Physiology, IKERBASQUE, Basque Foundation for Science, Faculty of Medicine and Dentistry, University of the Basque Country, Leioa, Spain

Received 21 February 2014; Revised 23 April 2014; Accepted 24 April 2014

DOI: 10.1002/pro.2483

Published online 28 April 2014 proteinscience.org

Abstract: The folding of most integral membrane proteins follows a two-step process: initially, individual transmembrane helices are inserted into the membrane by the Sec translocon. Thereafter, these helices fold to shape the final conformation of the protein. However, for some proteins, including Aquaporin 1 (AQP1), the folding appears to follow a more complicated path. AQP1 has been reported to first insert as a four-helical intermediate, where helix 2 and 4 are not inserted into the membrane. In a second step, this intermediate is folded into a six-helical topology. During this process, the orientation of the third helix is inverted. Here, we propose a mechanism for how this reorientation could be initiated: first, helix 3 slides out from the membrane core resulting in that the preceding loop enters the membrane. The final conformation could then be formed as helix 2, 3, and 4 are inserted into the membrane and the reentrant regions come together. We find support for the first step in this process by showing that the loop preceding helix 3 can insert into the membrane. Further, hydrophobicity curves, experimentally measured insertion efficiencies and MD-simulations suggest that the barrier between these two hydrophobic regions is relatively low, supporting the idea that helix 3 can slide out of the membrane core, initiating the rearrangement process.

Keywords: membrane protein; translocon recognition; protein folding; hydrophobicity; molecular dynamics

Additional Supporting Information may be found in the online version of this article.

Grant sponsor: Swedish Research Council, SSF (the Foundation for Strategic Research, Science for Life Laboratory the EU 6th Framework Program; GeneFun project; A.E., S.C., and M.V.); Grant number: LSHG-CT-2004-503567; Grant sponsor: 7th framework (EDICT project); Grant number: FP7-HEALTH-F4-2007-201924; Grant sponsor: Carl Trygger foundation (S.C.); Grant sponsors: Finnish Academy and the Sigrid Juselius Foundation (A.K. and N.A.); Grant sponsors: Sigrid Juselius Foundation and Tor, Joe and Pentti Borg Foundation (Excellent Computing Facilities).

*Correspondence to: Arne Elofsson; Department of Biochemistry and Biophysics Science for Life Laboratory, Stockholm University, SE-171 21 Solna, Sweden. E-mail: arne@bioinfo.se

Introduction

α -helical integral membrane proteins are essential for signaling, transport, energy production, and catalysis. The majority of α -helical membrane proteins fold following a two-stage process.¹ First, sufficiently hydrophobic segments are inserted into the membrane by the Sec translocon^{2,3} thereafter the protein folds. When a segment is sufficiently hydrophobic, it is recognized by the Sec-translocon^{2,4,5} and the orientation of the segment is primarily guided by the preference of positively charged residues in cytosolic loops.⁶ The initial recognition is followed by the less well-studied assembly of transmembrane

segments, binding of cofactors and formation of reentrant regions.⁷

Although the folding process is less well understood recent studies have highlighted that the folding process can in fact be remarkably complicated. In Bacteriorhodopsin, the folding transition state is not reached until the second and last (seventh) helix interact.⁸ Further, addition of positively charged residues can completely flip EmrE⁹ as well as most of the N-terminal half of LacY changes orientation in response to altered lipid composition.¹⁰ In cystic fibrosis transmembrane conductance regulator the integration of transmembrane helices proceeds in an unexpected order, the first transmembrane helix is integrated into the membrane only after the second transmembrane helix has been inserted.¹¹ These observations indicate that hydrophilic regions might pass through the membrane during folding.

The cost associated with hydrophilic regions passing through the membrane during these large-scale rearrangements could potentially be overcome by the utilization of external machineries, such as the translocon.¹² However, the membrane is not a uniform hydrophobic slab, but rather dynamic, and at least partly permitting the passage of polar groups. Indicative of this is how charged cell penetrating peptides,^{13,14} pore forming peptides,¹⁵ and some C-tail anchored proteins^{16,17} can enter the membrane spontaneously. The ability of polar groups to draw lipid head-groups and water deep into the core may provide a mechanism for their entry to the membrane.^{18,19}

A particular illustrative example for large-scale rearrangements is Aquaporin 1 (AQP1). Aquaporins forms water-soluble pores in biomembranes and in addition to the six transmembrane helices they contain two reentrant regions.²⁰ These two regions come together to almost form a seventh helix. Antibody epitope experiments in *Xenopus oocytes* demonstrated that AQP1 insert initially as a four-helix intermediate and only later folds into its final structure.²¹ In this intermediate, helices 2 and 4 are not inserted in the membrane, and consequently helix 3 is inserted in an inverted orientation,²¹ see Figure 1. Based on experiments in mammalian cells, the existence of the four-helix intermediate was initially questioned,²³ but this contradiction has been explained by the observation that the intermediate is less stable in mammalian cells.²⁴ In contrast, the close homolog Aquaporin 4 (AQP4) follows the conventional folding pathway, where each transmembrane segment is cotranslationally inserted into the membrane.²¹

To understand the sequence features causing the differences in folding pathways between AQP1 and AQP4 both proteins have been studied by truncation-reporter experiments in dog pancreatic microsomes.²² The most notable differences are helix

2 in AQP1 is less hydrophobic as it contains two polar residues, Asn49 and Lys51.²² When AQP1 helix 2 is not integrated into the membrane helix 3 is inserted in an inverted orientation, see Figure 1. The positive inside effect then prevents the integration of helix 4, as the C-terminal loop contains four lysines.²³ In addition, the loops flanking helix 3 have been suggested to play a role for its orientation.²²

In this study, we aim to shed some light on the folding process of AQP1. Based on our earlier observation that large-scale shifts are not infrequent in helical membrane proteins,²⁵ we propose that helix 3 can shift out of the membrane core and bring the preceding R1-H3 loop into the membrane, see Figure 1. We propose that this “R1-H3 shift” serves as a first step in AQP1 folding, followed later by additional events. Using a combination of experimental and computational techniques, we find that the “R1-H3 shift” is a feasible first step in AQP1 folding.

Results and Discussion

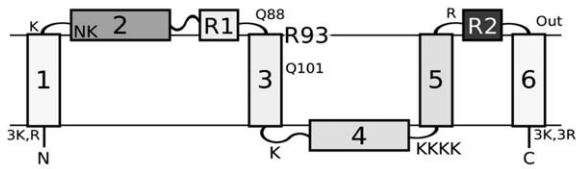
Here, we show that the “R1-H3 shift” is feasible and could serve as a first step in the folding of AQP1. In this model, the third transmembrane helix of AQP1 shifts out of the membrane core and the preceding “R1-H3 loop” is brought into the membrane. We show that the R1-H3 loop is sufficiently hydrophobic to reside in the membrane and that the energetic cost of the shift is consistent with the model. In contrast, the corresponding regions in AQP4 do not have these characteristics.

The R1-H3 loop is more hydrophobic in AQP1 than in AQP4

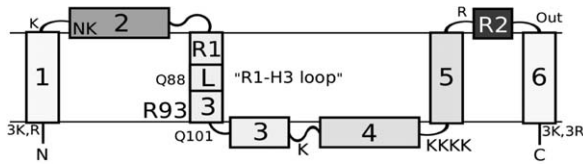
The hydrophobicity profiles of AQP1 and AQP4 protein families show the conservation of hydrophobicity profiles within each family but differs between the two families, see Figure 2. In AQP1, helix 2 is less hydrophobic and a hydrophobic segment ($\Delta G_{\text{pred}} \approx 0$ kcal/mol) is present just before helix 3. In AQP4, this segment is less hydrophobic ($\Delta G_{\text{pred}} \approx 4$ kcal/mol). This hydrophobic segment contains the helical section of reentrant region 1, the loop between the reentrant region and helix 3, and the N-terminal part of helix 3. Below we will refer to this region as the “R1-H3 loop.” The hydrophobicity of the R1-H3 loop indicates that this region might insert into the membrane. The hydrophobic barrier between helix 3 and the R1-H3 loop is relatively low ($\Delta G_{\text{pred}} \approx 3$ kcal/mol) and is mainly caused by a single residue, Arg93.

During the “R1-H3 shift” Arg93 has to cross the membrane from the luminal side to the cytosolic side, see Figure 1. Further, the positive inside rule would favor the rearrangement and support the “R1-H3 shift” hypothesis, which would serve as the first step in AQP1 folding.

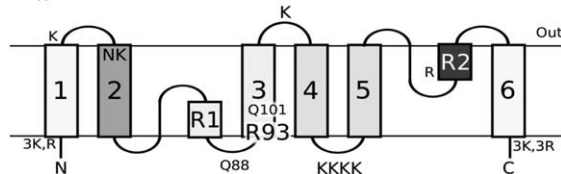
Aqp1 intermediate



Suggested H3 - R1 shift



Aqp1 structure



Aqp4

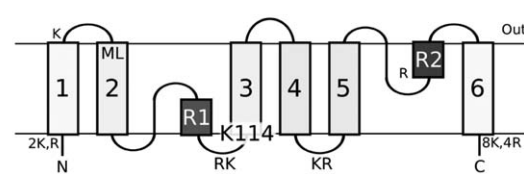


Figure 1. An overview of the topologies of AQP1 and AQP4 and the proposed “R1-H3 shift.” The proposed folding pathway for AQP1 is shown next to the topology of AQP4. All positively charged residues are shown. The gray shading roughly depicts the hydrophobicity of each segment to highlight the differences in hydrophobicity of TM2 and R1 between AQP1 and AQP4. The location of Asn49 and Lys51 in AQP1 helix 2 and the corresponding Met70 and Leu72 in AQP4 are also depicted. These residues are responsible for the hydrophobicity differences between the second helices.²² AQP1 is initially inserted into the membrane as a four-helix intermediate and later folds into its final six-helix topology.²¹ This requires the reorientation of helix 3. Here, we propose that helix 3 may spontaneously shift out of the membrane core (the R1-H3 shift), initiating the folding, despite the presence of polar residues (Arg93, Glu88, Glu101). Helix 3 in AQP4 contains three positively charged residues at its N-terminal side causing an orientational preference not present in the corresponding positions in AQP1.

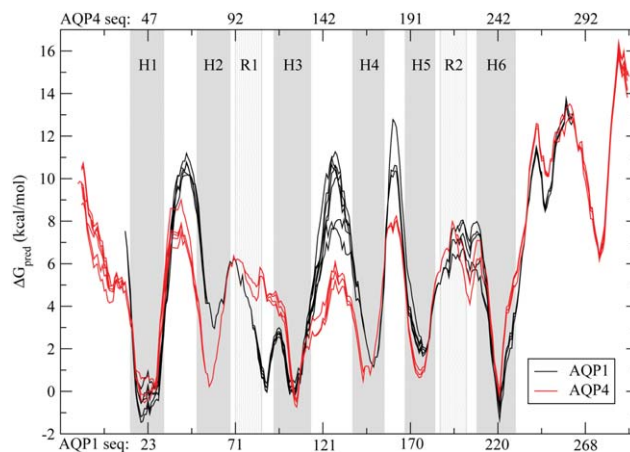


Figure 2. Hydrophobicity plots for aligned AQP1 and AQP4 protein sequences. Transmembrane helices are shaded in dark gray and reentrant regions in light gray. Sequence numbering corresponding to *Homo sapiens* AQP1 is shown below the figure and the numbering corresponding to AQP4 from *Rattus norvegicus* is shown on top. The predicted free energy of insertion (ΔG_{pred}) for each residue was calculated using the Hessa scale.⁵ The hydrophobicity profiles are conserved in both families, but show a clear difference between the families. In AQP1, the R1-H3 loop is almost as hydrophobic as helix 3 and the barrier separating these regions is quite low.

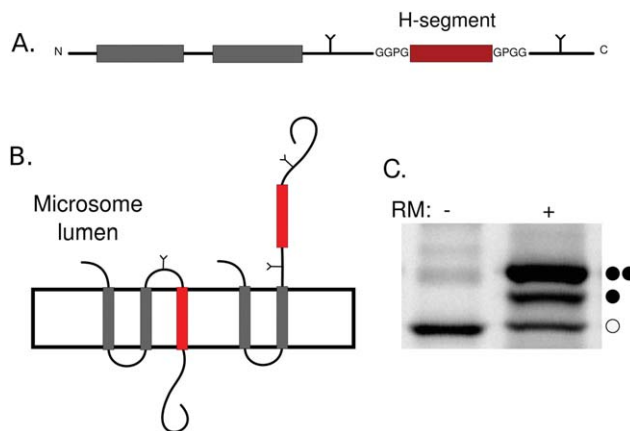


Figure 3. The leader peptidase (Lep) as a host protein and the *in vitro* expression in the presence of microsomes system. A) Segments from AQP1 and AQP4 were introduced as H-segments (depicted here in red) into the P2 domain of Lep, preceded by the two transmembrane helices (shown in gray) of wild type Lep. Lep is known to insert in a N_{lum} - C_{lum} orientation in rough microsomes. Asn-Xaa-Thr glycosylation sites were introduced on both sides of the H-segment. B) As glycosylation by the oligosaccharyl transferase only occurs in the micrososome lumen, the topology of a construct can be deduced from the number of glycans added to the protein. Here, singly glycosylated species arise from proteins with the H-segment inserted into the membrane whereas double glycosylated species arise from a translocated H-segment. C) An example of *in vitro* translation in the absence (-) and presence (+) of microsomes. Each glycan adds around 2 kDa to the molecular mass of the protein allowing their separation on SDS-PAGE. Here, nonglycosylated, single and double glycosylated protein species are indicated with open circles, one filled and two filled circles respectively. In this example, about 75% of the protein is doubly glycosylated.

In AQP1 the R1-H3 loop can be inserted into the membrane

A well-established *in vitro* glycosylation assay was used to identify segments in AQP1 and AQP4 that can be recognized by the translocon.^{5,26} Glycosylation can only occur in the micrososome lumen and can, therefore, be used as a topology marker. The insertion efficiencies of potential transmembrane helices can be determined by separating constructs with different number of attached glycans on SDS-PAGE, see Figure 3.

Insertion efficiencies of the R1-H3 loop (Ala78-Ala100), helix 3 (Ala94-Thr116) and the least hydrophobic segment between them (Leu84-Ile106) in AQP1 and corresponding segments from AQP4 were tested. In Figure 4, the experimental (ΔG_{exp}) values are shown together with the calculated hydrophobicity values (ΔG_{pred}). Given the experimental limitations, the predicted and experimental values are in good agreement. In AQP1, both the R1-H3 loop and helix 3 insert well, while in AQP4 only helix 3 is recognized by the translocon.

Translocon recognition was also tested using longer segments. These all start before the R1-H3 loop and include various truncations of helix 3. In general, these long segments inserts slightly better than the shorter segments, see Table I. In AQP1, but not in AQP4, the segment truncated at Ala100 that only includes six residues of helix 3 is inserted well, that is, the R1-H3 loop is efficiently recognized by the translocon in AQP1.

Identifying the translocon-recognized segments

Next, we aimed to determine the exact boundaries for the translocon-recognized segments in AQP1 using Minimal Glycosylation Distance Mapping (MGD),²⁷ see Figure 5. Two different constructs were studied: His69-Gly125, which contains the R1-H3 loop and the full-length helix 3, and His69-Ala100, which only contains six residues from helix 3.

In the longer construct, the glycosylation mapping identifies Ala94 to be the first membrane embedded residue and Val103 to be the last, see Figure 5. The N-terminus is in perfect agreement with the membrane boundary found in the crystal structure of AQP1 as defined in the PDBTM database,²⁸ but the helix is truncated at its C-terminus. In the shorter construct, the identified membrane region is shifted towards the N-terminus, spanning residues Ser86 to Tyr97. The C-terminus is located at the position expected for the recognition of the R1-H3 loop, but also this helix appears shorter than what is expected for a transmembrane helix.

One possible explanation for these unexpectedly short transmembrane regions could be that the segments are located in multiple membrane locations. They may be able to slide like a piston from one side of the membrane to the other. Then, when performing MGD mapping, the glycosylation could kinetically trap a state shifted towards one of the sides. Thereby, when mapping the C-terminus it would be shifted, and the helix appear to be shorter. The

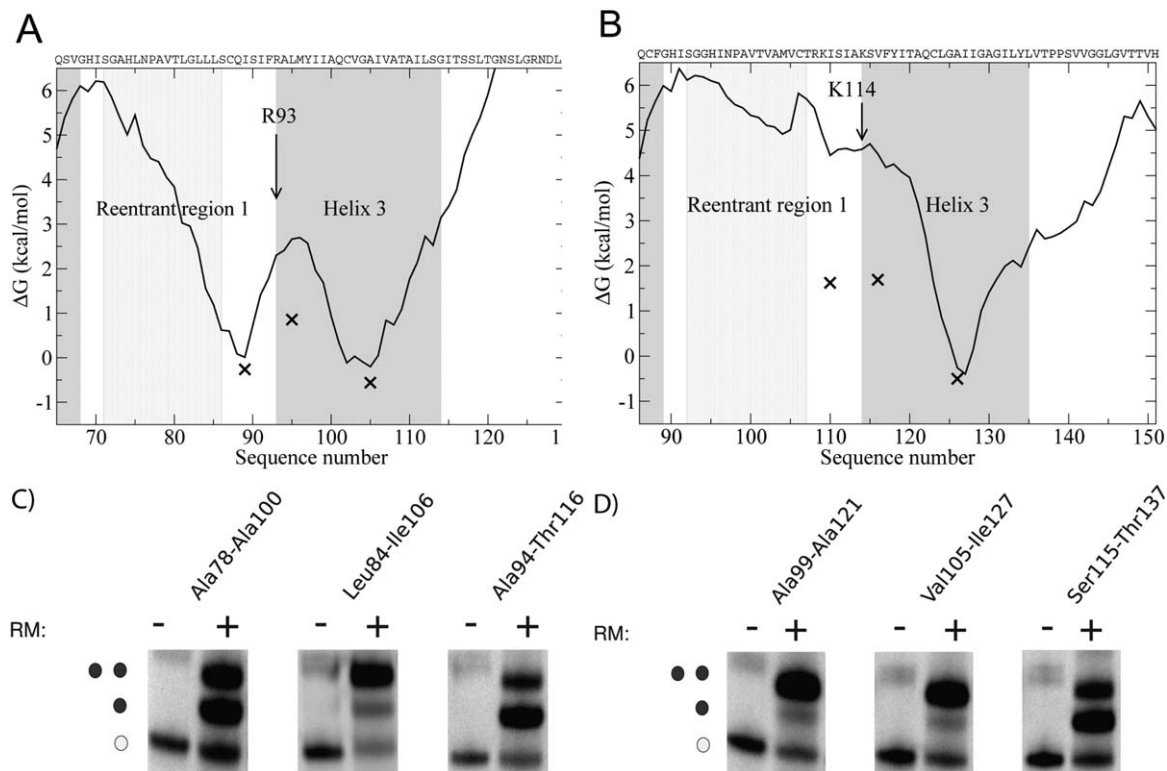


Figure 4. Experimentally determined insertion efficiencies compared to calculated insertion efficiencies. ΔG_{exp} values are plotted against the central position of the 23 residues long peptide. The curves represent the hydrophobicity as measured by ΔG_{pred} . Helices are shown with gray and reentrant region with a light gray background. A) In AQP1, both helix 3 and the R1-H3 loop area can be recognized by the translocon as independent membrane segments. In addition, the barrier is relatively low, which supports the possibility of a shift. B) In AQP4, only helix 3 is efficiently recognized as a transmembrane segment by the translocon. C) Representative SDS-page gels for AQP1 constructs expressed *in vitro*. D) Representative SDS-page gels for AQP4 constructs expressed *in vitro*.

identified short membrane regions are not recognized by the translocon, see Table I. This demonstrates that while the termini of these segments can reside within the membrane one at a time, they can-

not simultaneously be inside the membrane. Hence, a piston-like motion seems likely to occur, and when the glycosylation site is modified, the peptide is trapped.

Table I. Insertion Efficiencies, Experimentally Measured and Predicted Free Energies for Segments from AQP1 and AQP4

Construct	Length	Hydrophobic center	Inserted	ΔG_{exp}	ΔG_{pred}
Aquaporin 1					
His69-Met96	28	89	45%	0.12	0.85
His69-Ala100	32	91	80%	-0.83	-0.05
Ala78-Ala100	23	91	61%	-0.26	0.01
Ser86-Tyr97	11	92	6%	1.7	4.9
Leu84-Ile106	23	96	18%	0.92	2.70
Ala94-Val103	11	100	7%	1.6	4.5
Ala94-Thr116	23	106	72%	-0.56	-0.20
His69-Gly125	57	107	87%	-1.14	-0.20
Aquaporin 4					
His90-Ala113	24	105	15%	1.04	3.80
His90-Phe117	28	105	15%	1.04	3.80
His90-Ala121	32	111	17%	0.95	3.80
Ala99-Ala121	23	111	6%	1.68	4.45
Val105-Ile127	23	117	5%	1.69	4.48
Ser115-Thr137	23	127	69%	-0.48	-0.30
His90-Thr137	60	127	80%	-0.83	-0.53

The central position of the most central residue in the most hydrophobic segment is shown in column 3.

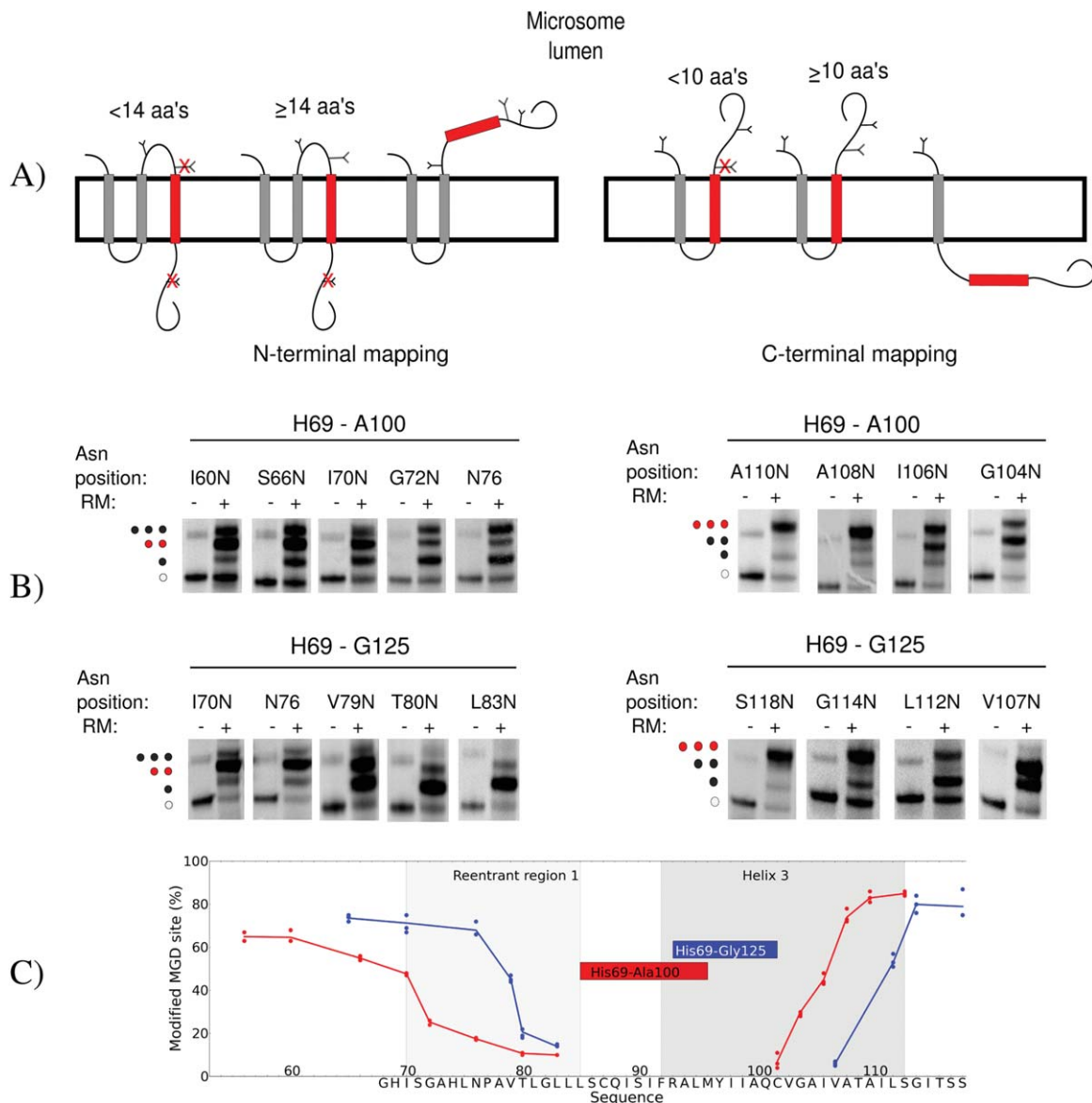


Figure 5. MGD of the N-terminal and C-terminal ends of transmembrane domains of His69-Gly125 and His69-Ala100 from AQP1. A) N-terminal mapping is shown to the left and C-terminal mapping to the right. In MGD, a third glycosylation site (MGD-site) is placed either before or after the H-segment. The position of the MGD-site is placed at different distances from the transmembrane region. The entire construct is expressed *in vitro* and the fraction of glycosylation at the MGD-site is measured. When approximately 50% of the MGD-sites are modified, that position is known to reside ≈ 14 residues before the N-termini of the membrane embedded region and ≈ 10 residues of its C-termini. B) The SDS-page gels show MGD-mapping for the two constructs. The position of the MGD-sites are indicated on top of the gels with the position corresponding to where the H-segments are embedded into the membrane marked in red. C) The glycosylation efficiency of the MGD-site is plotted against its position. The R1 and H3 regions are marked with light and dark gray shading, while the red and blue boxes represent the transmembrane helices as determined by the MGD-mapping for His69-Ala100 and His69-Gly125, respectively. The sequence of His69-Gly125 is presented at the X-axis.

Understanding the mechanisms enabling the R1-H3 shift

According to our experiments, the hydrophobic barrier between reentrant R1-H3 loop and H3 in AQP1 is ≈ 0.9 kcal/mol, see Figure 4 and Table I. This low barrier supports the possibility of a spontaneous R1-H3 shift, which involves Arg93 crossing the mem-

brane. To obtain insights into the molecular details of this transition, a series of molecular dynamics simulations were performed where the AQP1 R1-H3 peptide was restrained to different positions in the membrane, see Figure 6.

When either the R1-H3 loop or helix 3 are located at the membrane center, the long side-chain

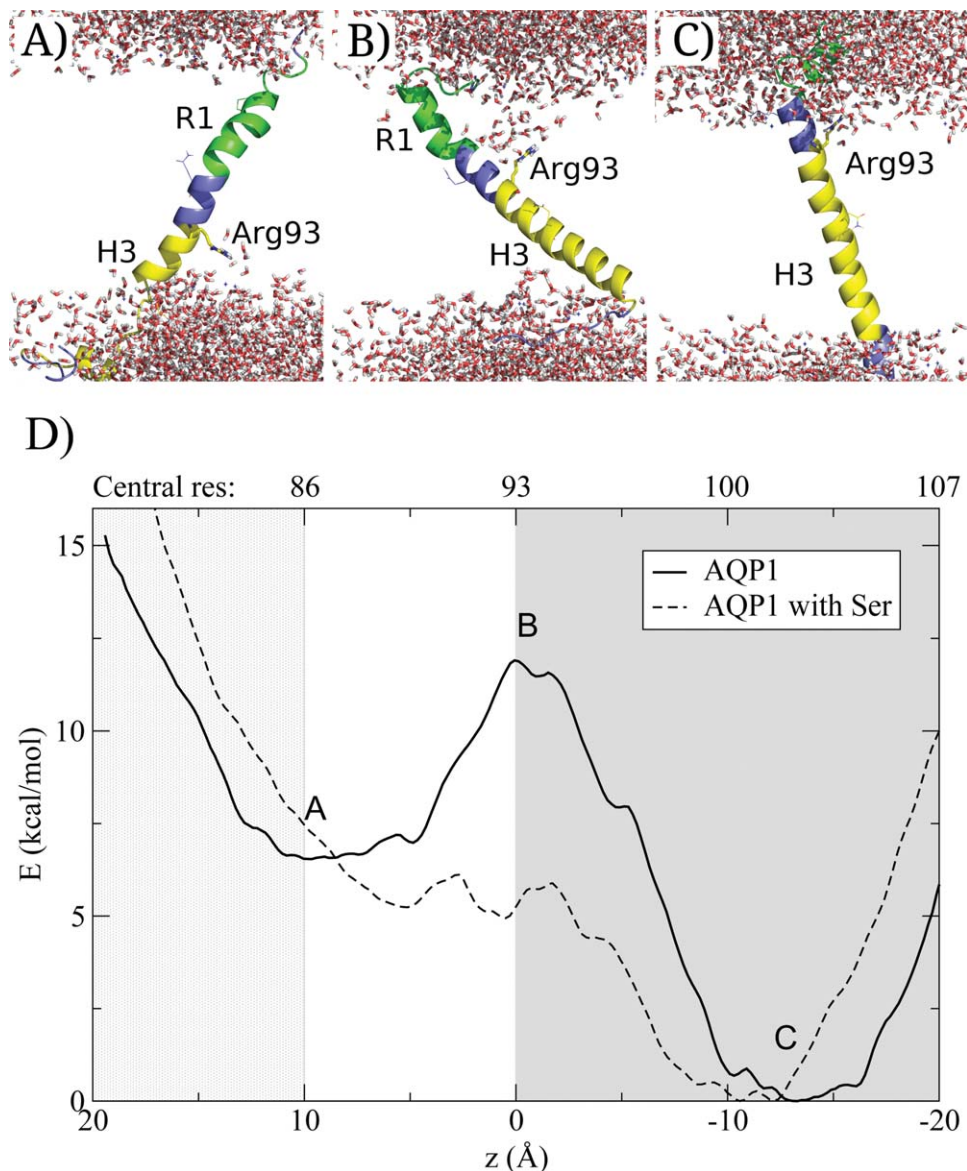


Figure 6. A–C) Snapshots from the simulation of the AQP1 R1–H3 segments with Arg93 placed at different positions in the membrane. Arg93 is depicted as a stick model. Gln88, Gln101, and Pro77 (that caps the reentrant region helix) are shown as lines. The helix 3 is drawn in yellow, loops in blue and R1 in green. Water molecules are depicted as stick models and no lipid molecules are shown for clarity. A) R1–H3 region in the membrane, B) Arg93 in the middle of the membrane, C) Helix 3 located in the middle of the membrane. D) Calculation of the potential mean force from umbrella samplings of the AQP1 R1–H3 segment. The mean force curves show two minima corresponding to when helix 3 or R1–H3 loop are in the membrane. The position where the snapshots are taken are marked with letters. The barrier corresponds Arg93 at the membrane. When serine analogs are added to the membrane, the barrier is decreased to near biological level. The letters A–C refer to the structural images. The number corresponding to the residue that located in the center of the membrane is shown above the plot. H3 is shown in gray and R1 in light gray.

of Arg93 snorkels toward one of the membrane interfaces. However, when Arg93 is in the center of the membrane, the membrane becomes distorted and water enters the membrane, as has been seen in earlier studies.^{29,30} Further, to avoid the energetic cost of dissolving hydrophobic regions into the surrounding water, the peptide tilts and brings the hydrophobic segment of helix 3 into the membrane. This might further lower the cost of the barrier.

Further, potential of mean force (PMF) calculations were used to estimate the free energy cost of insertion from the simulations. As expected for AQP1, the profile contains two clear minima, corresponding to the R1–H3 loop and helix three, Figure 6(D). The barrier between these minima corresponds to when Arg93 is in the center of the membrane.

The general shape of the PMF curve is similar to what is observed experimentally but the energy

barriers are higher. This is a well-known phenomenon³¹ and in accordance with earlier studies.^{3,29} The discrepancy has been explained by the lowered polarity of the translocon interior^{31,32} or by increased polarity caused by membrane proteins.^{33,34} To approximate for polar residues within the membrane, simulations were also performed with 20 serine analogs located in the membrane. In this system the barrier is lowered, indicating that the R1-H3 shift may be plausible in real cytoplasmic membranes.

Implications for folding of AQP1

The results presented above suggest a spontaneous shift of helix 3 during AQP1 folding. When helix 3 moves out of the membrane core the R1-H3 loop integrates into the membrane. The positive inside rule would favor such a shift, as Arg93 would move to the cytoplasmic side. Also, Arg93 may form stabilizing interactions with other residues in AQP1 during the shift, in particular with Glu17 from helix 1. The reinsertion of helix 3 together with helix 4 would then be sufficient to bring helix 3 into its correct orientation, see Figure 1. How the hydrophilic H3-H4 loop could pass through the membrane is not clear. However, AQP1 is a channel and the reorientation process requires the presence of helices 5 and 6.²¹ In addition, the final topology would require refolding of helix 2 and the reentrant regions. It could be imagined that these regions enter the membrane jointly.

The reorientation of AQP1 is less efficient in a cell free system than in *Xenopus oocytes* indicating that while the R1-H3 shift could occur spontaneously, the later stages of rearrangements may depend on the presence of additional cellular machineries.²¹ The translocon has been suggested to play a key role in the reorientation of AQP1.¹² Alternatively, the translocating chain associated membrane protein (TRAM), could also be involved, as it has previously been shown to aid the insertion of charged helices.³⁵ Conversely, LacY has been shown to be capable of dramatic reorientation, including change in orientation for transmembrane domains and posttranslational insertion of a transmembrane helix, without any other cellular factors except the lipid composition of the membrane.⁴⁶ Anyhow, extensive additional studies are required to understand how the folding could proceed after the R1-H3 shift.

Conclusions

The folding of AQP1 does not follow the traditional two-stage folding process. In AQP1, helix 3 inverts its orientation in the membrane after the initial insertion, whereas this does not occur in the homologous AQP4. Consequently, AQP4 does not show any of the characteristics listed below.²¹ Here, we propose a mechanism for the initial steps in the folding of AQP1; First, helix 3 is shifted out of the mem-

brane core resulting in the preceding regions to be pulled into the membrane, this is followed by a reinsertion of helix 3 in its correct orientation, see Figure 1. We present three observations supporting this idea. First, we noted an additional conserved hydrophobic segment, the R1-H3 loop, next to helix 3, see Figure 2. We show that this region can be integrated efficiently into the membrane by the translocon, see Table I and Figure 4. Second, experimental, predicted, and simulated hydrophobicity values implicate a relatively low barrier between helix 3 and the R1-H3 loop, see Figure 2, 4, and 6. Also experimental minimum glycosylation distance mapping suggests that several alternative segments can be recognized by the translocon in the R1-H3 region and that this region might undergo a piston like motion. Finally, the positive inside rule would also favor the shift as Arg93 would move to the cytoplasmic side of the membrane, see Figure 1.

Methods

Alignments and ΔG plots

All members of the Aquaporin 1 and 4 families were extracted from Swissprot³⁶ in November 2011. A multiple sequence alignment of all these protein sequences was done using kalign³⁷ with default parameters. The hydrophobicity of individual segments was estimated by the predicted free energy of insertion (ΔG_{pred}) calculated from the biological hydrophobicity scale.⁵ For each residue in the hydrophobicity profiles, the optimal window length ranging between 19 and 23 residues was used.

Enzymes and chemicals

Unless otherwise stated, chemicals were obtained from Sigma-Aldrich (St. Louis, MO), oligonucleotides were obtained from MWG Biotech AG (Ebersberg, Germany), and all enzymes were from Fermentas (Burlington, Ontario, Canada), except Phusion DNA polymerase that was obtained from Finnzymes OY (Espoo, Finland). The plasmid pGEM-1 and the TNT[®] SP6 Quick Coupled Transcription/Translation System were from Promega Biotech AB (Madison, WI). [³⁵S]Met was bought from Perkin Elmer (Boston, MA) and the column washed dog pancreas rough microsomes were from tRNAprobes (College Station, TX). The EndoH assay kit was from New England Biolabs (Ipswich, MA). The Qiaprep Mini-prep Plasmid Purification kits from QIAGEN (Hilden, Germany) were used for plasmid purifications. E.Z.N.A Cycle Pure and Gel Extraction kits from Omega Bio-Tek (Norcross, GA) were used during post-PCR manipulation.

DNA manipulation

The *lepB* gene had previously been introduced into the pGEM-1 vector under the control of the SP6-

promoter³⁸ and with the context 5' of the initiator codon changed to a Kozak consensus sequence.³⁹ To allow Lep to "host" other protein segments, SpeI and KpnI restriction recognition sites had been introduced in the sequence encoding the middle of the P2-domain (LepI). In all constructs, two glycosylation sites are placed on each side of the H-segment.³ To insulate each sequence from the Lep sequence, all segments contain both N-terminal and C-terminal GGPG...GGPG flanks.

Double-stranded oligonucleotides encoding the different protein segments from AQP1 (*Homo sapiens*) and AQP4 (*Rattus norvegicus*) were introduced into the *lepB* gene as SpeI-KpnI-fragments of amplified PCR fragments using primers complementary to the 5' and 3' ends of the selected part of the gene (for exact amino acid sequences for these segments, see Table I. Both the vector and the PCR fragments were digested with SpeI and KpnI (Fermentas) separated on agarose gel and fragments of correct size were excised from gel and purified (E.Z.N.A. Gel Extraction kit). PCR fragments were ligated to the vector carrying the *lepB* gene using Rapid DNA Ligation Kit (Fermentas).

Point mutations

For MGD in AQP1 additional glycosylation sites were introduced into the sequence, using His69-Ala100 and His69-Gly125 as templates. To determine the first N-terminal residue recognized by the translocon, the H-segments were introduced into LepI and a series of constructs where the third glycosylation site was introduced at different positions downstream of Arg93 were made, see Figure 5(A). For determining the last membrane embedded residue at the C-termini, the constructs were introduced to LepII and again, a series of constructs with a third glycosylation site at varying distances upstream were made, Figure 5(B).

For each glycosylation position, the native amino acids in the sequence were exchanged into Asn-Ser-Thr. We chose to use the same glycosylation site sequon even if this introduces larger changes in the amino acid sequence of the H-segments to prevent fluctuations in glycosylation efficiency.^{40,41} All DNA modifications were confirmed by sequencing of the plasmid DNA at Eurofins MWG Operon.

Expression in vitro

Constructs in pGEM-1 were transcribed and translated in the TNT SP6 Quick Coupled System from Promega. A master mix containing [³⁵S]-methionine (5 μCi) and lysate were mixed together in such a way that the amount of lysate is ten times the volume of [³⁵S]-methionine. Master mix (5.5 μl) was then added to 100 ng DNA. For positive reactions, the master mix was supplemented with dog pancreas column washed rough microsomes, in an

amount that would yield at minimum 80 % targeting. All samples were incubated at 30°C for 90 min. For long segments, the results did not differ more than 5% points and therefore only doublets were made. However, as the variations were greater for AQP1 short segments, up to seven replicates were made. For MGD-mapping, three replicates were made for each construct, with variation typically within 7% points.

Separation and analysis of expressed proteins

Translated proteins were separated by SDS-PAGE and visualized with a Fuji FLA-3000 phosphoimager (Fujifilm, Tokyo, Japan) with the ImageReader V1.8J/Image Gauge V 3.45 software (Fujifilm). The MultiGauge software was used to create one-dimensional intensity profiles for each lane on the gels, where the triply glycosylated proteins yield a higher molecular weight (+6 kDa), doubly glycosylated (+4 kDa) band and singly glycosylated proteins (+2 kDa), as compared to the nonglycosylated protein. The differently glycosylated proteins are denoted with filled circles in the figures and the nonglycosylated protein with unfilled circles. Peak areas were then analyzed using the multi-Gaussian fit program from the Qtiplot software package (<http://www.qtiplot.ro/>).

The apparent membrane insertion free energies for AQP1 and AQP4 segments

The apparent membrane insertion free energies ΔG_{exp} for the H-segments (AQP1 and AQP4 segments given in Table I) were calculated as follows. The fraction of singly (fx1) and doubly (fx2) glycosylated species can be used to calculate the apparent equilibrium constant $K_{\text{exp}} = \frac{\text{fx1}}{\text{fx2}}$ for a given H-segment. The K_{exp} value can be converted into an apparent free energy difference between the noninserted and inserted state: $\Delta G_{\text{exp}} = -RT \ln K_{\text{exp}}$, where R is the gas constant and T is the temperature in Kelvin. The accuracy of ΔG_{exp} determination is good between the interval of -1.5 and 1.0 kcal/mol.⁵

Minimal glycosylation distance mapping

In MGD experiments, the fraction of proteins that were singly, doubly, and triply glycosylated was measured. Nonglycosylated proteins were not included, as they had not been targeted to the microsomal membranes.

For the N-terminal mapping, singly glycosylated proteins represent the state when the H-segment is integrated into the membrane and the MGD-site is too close to the membrane to be modified by the Oligosaccharyltransferase. For constructs that generate a larger fraction of doubly glycosylated proteins, the MGD-site is far enough from the membrane to get efficiently modified. H-segments that do not integrate into the membrane carry three glycans, see

Figure 5. For the C-terminal mapping, doubly glycosylated proteins have the H-segment integrated into the membrane but the MGD-site is too close to the membrane. When the MGD-site is sufficiently distant a three-glycan form appear.

It should be noted that in the shorter construct the polar residues at the glycosylation site disturb the membrane insertion of the R1-H3 loop causing the short construct to not reach the same level of double glycosylation as in the longer construct, Figure 5. In addition, when the MGD-site is closer than 13 residues to Arg93, the segment is poorly recognized by the translocon as evident from gel images where a sudden increase of noninserted (three-glycan form) can be seen, Figure 5(C).

Endoglycosidase H digestion

It was observed that some of the His69-Gly125 constructs in MGD-experiments appeared to be cleaved by Signal Peptidase resulting in multiple bands for some constructs, see Supporting Information Figure S1. As the fraction of the constructs that are cleaved varies between differently glycosylated constructs, it is necessary to identify which bands correspond to each glycosylation state.

To assess the correct cleaved fragments to their respective glycosylated protein species, an Endoglycosidase H (EndoH) assay was²⁶ carried out. Here, 6 μ l of translation products were mixed with resuspended 1 μ l denaturing buffer (10 \times) and 3 μ l distilled water. After mixing, 2 μ l of G5 reaction buffer (10 \times) and 7 μ l of distilled water were added. Finally, either 1 μ l of Endo H (500,000 units/ml) or dH₂O (mock sample) was added. The samples were incubated at 37°C for 1 h. From here on, the samples were treated as all other *in vitro* expressed constructs. During analysis, to calculate the ratio of membrane embedded transmembrane regions the cleaved and noncleaved forms were measured independently and the fractions noncleaved and cleaved fragments were added.

Molecular dynamics simulations

MD simulations were performed using Gromacs 4.5.5⁴² with the Berger lipid force field.⁴³ Equilibrated 1-Palmitoyl-2-oleoylphosphatidylcholine (POPC) and 1-Palmitoyl-2-oleoylphosphatidylserine (POPS) in a 3:1 mixture were used in the membrane bilayer. POPC was chosen, because it is widely used in MD simulations and its parameters are well optimized and POPS was included to represent anionic lipids that may interact with the cationic Arg93.

The length of AQP1 R1-H3 peptide was optimized by trial and error and the His69-Asn122 peptide was chosen. This peptide contains approximately an additional five residues on each side of the hydrophobic region. The peptide was built in an idealized helical conformation using the PyMOL Molecular Graphics

System, Version 0.99, DeLano Scientific, Palo Alto, CA, USA. The peptide was embedded into a membrane by program *g_membed*.⁴⁴ The resulting membrane consisted of 66 POPC and 22 POPS molecules.

In all molecular dynamics simulations, we used a 2 fs time step, LINCS constraints, 1.2 nm cutoffs (Coulomb, van der Waals and neighbor list), PME electrostatics, V-rescale temperature coupling to 323 K temperature and Parinello-Rahman pressure coupling to 1 bar pressure. A semi-isotropic temperature coupling was applied, where the pressure in the plain of the bilayer was coupled separately from the normal of the bilayer.

Forty one separate simulations were prepared with the R1-H3 segment positioned at different depth of the membrane. The starting position of each simulation differed by 0.1 nm. Each system was then solvated, neutralized by 21 sodium ions, minimized and equilibrated by a 1 ns simulation using position restraints (1000kJ mol⁻¹nm⁻²) for all protein atoms. Each simulation was sampled during a 20 ns simulations using position geometry at the direction of the Z-axis and a 1000kJ mol⁻¹nm⁻² force constant. The membrane center and C- α atoms for residues 92–94 were used as reference groups. The first 5 ns of each simulation were discarded. Each simulation was run twice. To ensure full coverage of the mean force histogram, a few additional windows were added around the central position. The weighted histogram analysis method (program *g_wham*⁴⁵) was used to extract the PMF curve.

It is well known that cellular membranes contain a large fraction of proteins. In simulations, when additional proteins are included in the membrane, the cost for hydrophilic residues to enter the membrane is lowered.³³ However, in our simulations it was not possible to add entire helices, as this would have required much longer simulations, which would be computationally too expensive. Instead 20 serine analogs (methanol) were added to the membrane and each simulation was run three times. The addition of serines was based on the assumption that up to half of the membrane content consist of proteins, half of the residues are exposed and a quarter of exposed residues are at least mildly polar, that is, 20 serine analogs roughly provides the same ratio of polar residues as found in real membranes.¹⁹ The topology of the serine analog was modified starting from the topology of serine and the atom type of CB was changed to CH3. Serine was chosen, as it is a mildly hydrophilic residue that can act both as a donor and acceptor in hydrogen bond. Further, it is rather frequent within membrane regions. Position restraints (1000kJ mol⁻¹nm⁻²) were also applied to the Z-coordinate of the serine CB atom.

Acknowledgments

Professor William Skach is kindly acknowledged for providing plasmids and harboring the genes for

AQP1 and AQP4, Dr. Linnea Hedin and Dr. IngMarie Nilsson for valuable advice regarding laboratory work, Prof. Peter Tieleman for lipid structures, topologies and force field parameters, Prof. Erik Lindahl for stimulating discussions, Dr. Justin Lemkul for instructive web tutorials and Dr. Sara Light for proofreading the manuscript. Mark Johnson from Åbo Akademi University has provided to AK and NA excellent computing facilities (funded by Sigrid Juselius Foundation and Tor, Joe and Pentti Borg Foundation) and availability to the Biocenter Finland infrastructure and to the Finnish Grid Infrastructure. The majority of simulations were performed at the PDC center for high performance computing and we are also grateful for additional computational resources given to us by SNIC at NSC and Uppmax.

References

1. Popot J, Engelman D (1990) Membrane protein folding and oligomerization: the two-stage model. *Biochemistry* 29:4031–4037.
2. Heinrich S, Mothes W, Brunner J, Rapoport T (2000) The sec61p complex mediates the integration of a membrane protein by allowing lipid partitioning of the transmembrane domain. *Cell* 102:233–244.
3. Hessa T, Kim H, Bihlmaier K, Lundin C, Boekel J, Andersson H, Nilsson I, White S, von Heijne G (2005) Recognition of transmembrane helices by the endoplasmic reticulum translocon. *Nature* 433:377–381.
4. Van den Berg B, Clemons W, Jr, Collinson I, Modis Y, Hartmann E, Harrison S, Rapoport T (2004) X-ray structure of a protein-conducting channel. *Nature* 427:36–44.
5. Hessa T, Meindl-Beinker N, Bernsel A, Kim H, Sato Y, Lerch-Bader M, Nilsson I, White S, von Heijne G (2007) Molecular code for transmembrane-helix recognition by the sec61 translocon. *Nature* 450:1026–1030.
6. von Heijne G (1989) Control of topology and mode of assembly of a polytopic membrane protein by positively charged residues. *Nature* 341:456–458.
7. Engelman D, Chen Y, Chin C, Curran A, Dixon A, Dupuy A, Lee A, Lehnert U, Matthews E, Reshetnyak Y, Senes A, Popot J (2003) Membrane protein folding: beyond the two stage model. *FEBS Lett* 555:122–125.
8. Booth P (2012) A successful change of circumstance: a transition state for membrane protein folding. *Curr Opin Struct Biol* 22:469–475.
9. Seppala S, Slusky J, Lloris-Garcera P, Rapp M, von Heijne G (2010) Control of membrane protein topology by a single c-terminal residue. *Science* 328:1698–1700.
10. Bogdanov M, Xie J, Heacock P, Dowhan W (2008) To flip or not to flip: lipid-protein charge interactions are a determinant of final membrane protein topology. *J Cell Biol* 182:925–935.
11. Lu Y, Xiong X, Helm A, Kimani K, Bragin A, Skach W (1998) Co- and posttranslational translocation mechanisms direct cystic fibrosis transmembrane conductance regulator n terminus transmembrane assembly. *J Biol Chem* 273:568–576.
12. Skach W (2009) Cellular mechanisms of membrane protein folding. *Nat Struct Mol Biol* 16:606–612.
13. Madani F, Lindberg S, Langel U, Futaki S, Graslund A (2011) Mechanisms of cellular uptake of cell-penetrating peptides. *J Biophys* 2011:414729.
14. Herce H, Garcia A (2007) Cell penetrating peptides: how do they do it? *J Biol Phys* 33:345–356.
15. Iacovache I, Bischofberger M, van der Goot F (2010) Structure and assembly of pore-forming proteins. *Curr Opin Struct Biol* 20:241–246.
16. Borgese N, Fasana E (2011) Targeting pathways of c-tail-anchored proteins. *Biochim Biophys Acta* 1808:937–946.
17. Hegde R, Keenan R (2011) Tail-anchored membrane protein insertion into the endoplasmic reticulum. *Nat Rev Mol Cell Biol* 12:787–798.
18. Hristova K, Wimley W (2011) A look at arginine in membranes. *J Membr Biol* 239:49–56.
19. Illergard K, Kauko A, Elofsson A (2011) Why are polar residues within the membrane core evolutionary conserved? *Proteins* 79:79–91.
20. Murata K, Mitsuoka K, Hirai T, Walz T, Agre P, Heymann JB, Engel A, Fujiyoshi Y (2000) Structural determinants of water permeation through aquaporin-1. *Nature* 407:599–605.
21. Lu Y, Turnbull I, Bragin A, Carveth K, Verkman A, Skach W (2000) Reorientation of aquaporin-1 topology during maturation in the endoplasmic reticulum. *Mol Biol Cell* 11:2973–2985.
22. Foster W, Helm A, Turnbull I, Gulati H, Yang B, Verkman A, Skach W (2000) Identification of sequence determinants that direct different intracellular folding pathways for aquaporin-1 and aquaporin-4. *J Biol Chem* 275:34157–34165.
23. Dohke Y, Turner R (2002) Evidence that the transmembrane biogenesis of aquaporin 1 is cotranslational in intact mammalian cells. *J Biol Chem* 277:15215–15219.
24. Buck T, Skach W (2005) Differential stability of biogenesis intermediates reveals a common pathway for aquaporin-1 topological maturation. *J Biol Chem* 280:261–269.
25. Kauko A, Hedin L, Thebaud E, Cristobal S, Elofsson A, von Heijne G (2010) Repositioning of transmembrane alpha-helices during membrane protein folding. *J Mol Biol* 397:190–201.
26. Lundin C, Kim H, Nilsson I, White S, von Heijne G (2008) Molecular code for protein insertion in the endoplasmic reticulum membrane is similar for n(in)-c(out) and n(out)-c(in) transmembrane helices. *Proc Natl Acad Sci USA* 105:15702–15707.
27. Armulik A, Nilsson I, von Heijne G, Johansson S (1999) Determination of the border between the transmembrane and cytoplasmic domains of human integrin subunits. *J Biol Chem* 274:37030–37034.
28. Tusnady G, Dosztanyi Z, Simon I (2004) Transmembrane proteins in the protein data bank: identification and classification. *Bioinformatics* 20:2964–2972.
29. Dorairaj S, Allen T (2007) On the thermodynamic stability of a charged arginine side chain in a transmembrane helix. *Proc Natl Acad Sci USA* 104:4943–4948.
30. Vorobyov I, Allen T (2011) On the role of anionic lipids in charged protein interactions with membranes. *Biochim Biophys Acta* 1808:1673–1683.
31. Schow E, Freitas J, Cheng P, Bernsel A, von Heijne G, White S, Tobias D (2011) Arginine in membranes: the connection between molecular dynamics simulations and translocon-mediated insertion experiments. *J Membr Biol* 239:35–48.
32. Gumbart J, Chipot C, Schulten K (2011) Free-energy cost for translocon-assisted insertion of membrane proteins. *Proc Natl Acad Sci USA* 108:3596–3601.
33. Johansson A, Lindahl E (2009) Protein contents in biological membranes can explain abnormal solvation of

- charged and polar residues. *Proc Natl Acad Sci USA* 106:15684–15689.
34. Rychkova A, Vicatos S, Warshel A (2010) On the energetics of translocon-assisted insertion of charged transmembrane helices into membranes. *Proc Natl Acad Sci USA* 107:17598–17603.
 35. Martinez-Gil L, Perez-Gil J, Mingarro I (2008) The surfactant peptide KL4 sequence is inserted with a transmembrane orientation into the endoplasmic reticulum membrane. *Biophys J* 95:L36–L38.
 36. Bairoch A, Apweiler R (1996) The swiss-prot protein sequence data bank and its new supplement trembl. *Nucleic Acids Res* 24:17–21.
 37. Lassmann T, Frings O, Sonnhammer E (2009) Kalign2: high-performance multiple alignment of protein and nucleotide sequences allowing external features. *Nucleic Acids Res* 37:858–865.
 38. Johansson M, Nilsson I, von Heijne G (1993) Positively charged amino acids placed next to a signal sequence block protein translocation more efficiently in *escherichia coli* than in mammalian microsomes. *Mol Gen Genet* 239:251–256.
 39. Kozak M (1989) Context effects and inefficient initiation at non-AUG codons in eucaryotic cell-free translation systems. *Mol Cell Biol* 9:5073–5080.
 40. Mellquist J, Kasturi L, Spitalnik S, Shakin-Eshleman S (1998) The amino acid following an asn-x-ser/thr sequon is an important determinant of n-linked core glycosylation efficiency. *Biochemistry* 37:6833–6837.
 41. Shakin-Eshleman S, Spitalnik S, Kasturi L (1996) The amino acid at the x position of an asn-x-ser sequon is an important determinant of n-linked core-glycosylation efficiency. *J Biol Chem* 271:6363–6366.
 42. Hess B, Kutzner C, van der Spoel D, Lindahl E (2008) Gromacs 4: Algorithms for highly efficient, load-balanced, and scalable molecular simulation. *J Chem Theory Comput* 4:435–447. arXiv:<http://pubs.acs.org/doi/pdf/10.1021/ct700301q>, doi:10.1021/ct700301q. Available at: URL <http://pubs.acs.org/doi/abs/10.1021/ct700301q>.
 43. Berger O, Edholm O, Jahnig F (1997) Molecular dynamics simulations of a fluid bilayer of dipalmitoylphosphatidylcholine at full hydration, constant pressure, and constant temperature. *Biophys J* 72:2002–2013.
 44. Wolf MG, Hoefling M, Aponte-Santamaria C, Grubmuller H, Groenhof G (2010) g_membed: efficient insertion of a membrane protein into an equilibrated lipid bilayer with minimal perturbation. *J Comput Chem* 31:2169–2174.
 45. Hub JS, de Groot BL, van der Spoel D (2010) g_whams: free weighted histogram analysis implementation including robust error and autocorrelation estimates. *J Chem Theory Comput* 6:3713–3720.
 46. Vitrac H, Bogdanov M, Dowhan W (2013) In vitro reconstitution of lipid-dependent dual topology and postassembly topological switching of a membrane protein. *Proc Natl Acad Sci U S A* 110:9338–9343.